

Topologically protected excitons in porphyrin thin films

Joel Yuen-Zhou¹, Semion K. Saikin^{1,2}, Norman Yao³, and Alán Aspuru-Guzik^{1,2}

¹*Center for Excitonics, Research Laboratory of Electronics,
Massachusetts Institute of Technology, Cambridge, MA, USA.**

²*Department of Chemistry and Chemical Biology, Harvard University, Cambridge, MA, USA. and*

³*Department of Physics, Harvard University, Cambridge, MA, USA.*

The control of exciton transport in organic materials is of fundamental importance for the development of efficient light-harvesting systems. This transport is easily deteriorated by traps in the disordered energy landscape. Here, we propose and analyze a system that supports topological Frenkel exciton edge states. Backscattering of these chiral Frenkel excitons is prohibited by symmetry, ensuring that the transport properties of such a system are robust against disorder. To implement our idea, we propose a two-dimensional periodic array of tilted porphyrins interacting with a homogenous magnetic field. This field serves to break time-reversal symmetry and results in lattice fluxes that mimic the Aharonov-Bohm phase acquired by electrons. Our proposal is the first blueprint for realizing topological phases of matter in molecular aggregates and suggests a paradigm for engineering novel excitonic materials.

Upon interactions with light, molecules are promoted to excited states, typically referred to as molecular excitons [1] (hereafter referred to as excitons interchangeably). The efficient transport of energy across a molecular array via such excitons is one of the main goals in the design of solar cell devices [2]. This owes to the fact that excitons mediate energy transfer between incoming photons and the electrical current generated upon excited-state dissociation [3, 4]. In this context, tremendous efforts have been focused on organic photovoltaic materials, which have advantages in terms of production cost, chemical versatility, and enhanced absorption properties. However, an important drawback in such organic materials is the presence of a large amount of disorder [5, 6]. Indeed, static disorder arises from structural imperfections in the molecular aggregate which yield local perturbations to the on-site energies as well as to the couplings between molecules. Typically, such disorder induces Anderson localization of the single-particle exciton eigenstates [7], which significantly reduces transport. While such localizing effects can be partially compensated by the addition of vibrations which help untrap the exciton [8–10], a generic solution remains a challenge.

Our approach to this challenge draws upon ideas from the field of disordered electronic systems—in particular, from the phenomenology broadly termed as “quantum Hall effects” (QHEs) [11]. A hallmark of such quantum hall systems is that they exhibit delocalized current-carrying chiral edge modes. Specifically, the breaking of time-reversal symmetry (TRS) in these systems ensures that there are no counter-propagating modes to backscatter into [12]. Elegant extensions of these ideas include photonic setups [13–17] and topological insulators (TI)—materials that preserve TRS but whose edge modes are related to strong spin-orbit coupling [18–21]. We note that organometallic TIs have recently been suggested by Liu and coworkers [22–25], paving the way towards a wider and possibly cheaper group of materials that may exhibit these exotic phenomena.

Since QHEs have been posed in the context of electrons and photons, it is natural to inquire whether their excitonic analog exists. The present article answers this question positively, by explicitly constructing a minimal model of a Frenkel exciton porphyrin lattice which supports topologically protected edge states when it interacts with a magnetic field. Since this effort is already challenging by itself, we limit ourselves to cryogenic temperatures, and therefore, disregard effects of vibrational dephasing of excitons, which we shall study elsewhere. As far as we are aware, this is curiously the first work that addresses the joint effects of both *magnetic fields* and *coherence* in molecular exciton transport. Furthermore, this article is also the first example of topological phases in molecular excitons, and therefore, offers a novel approach to the design of a new generation of materials for more efficient energy harvesting and transport.

Description of the model

Description of the lattice.— Our setup consists of a two-dimensional periodic array of unsubstituted metalloporphyrins (hereafter referred to just as porphyrins), molecules with D_{4h} symmetry that maintain their planarity due to their metal centers [26, 27], and which are well known compounds in photovoltaic applications [28–30]. These porphyrins are arranged in a square lattice in the xy plane with a unit cell of area $s \times s$ (see Fig. 1a), where $s \sim \frac{1}{2} - 2$ nm. The lattice consists of two sublattices a and b , where the porphyrins are tilted out of the xy plane in ways that depend on two angles per sublattice, θ_i and φ_i ($i = a, b$), respectively. This two-dimensional lattice can in principle be realized by self-assembly techniques exploiting an already crystalline substrate [31–36], which in our case, shall be chosen to avoid exciton quenching processes (an insulating material fulfills this condition [37, 38]).

Using a Cartesian vector notation in the “lab” or array frame throughout the article, the a sites are located at positions $ns \equiv (n_x, n_y, 0)s$ for n_x, n_y integers, whereas the b sites are at $(n + \frac{1}{2})s = (n_x + \frac{1}{2}, n_y + \frac{1}{2}, 0)s$. We shall be concerned with the three lowest electronic states in each molecule, namely, its

*Electronic address: joelyuen@mit.edu

ground state $|g^{(i)}\rangle$, and its degenerate Q-band absorbing in the visible spectrum ($\omega_Q \sim 17350\text{cm}^{-1}$ [39]), consisting of the orthogonal states $|Q_X^{(i)}\rangle$ and $|Q_Y^{(i)}\rangle$ (we use capital labels for Cartesian coordinates for the molecular frame of each sublattice).

Due to the degeneracy of the Q-band, the states $|Q_X^{(i)}\rangle$ and $|Q_Y^{(i)}\rangle$ can be arbitrarily defined as long as their transition dipole moments with respect to $|g^{(i)}\rangle$ constitute an orthogonal set of vectors of equal magnitude d spanning the plane of each porphyrin. We denote the transition dipole operator for a porphyrin in sublattice i by $\mu^{(i)} = \mu_{Q_Xg}^{(i)}|Q_X^{(i)}\rangle\langle g^{(i)}| + \mu_{Q_Yg}^{(i)}|Q_Y^{(i)}\rangle\langle g^{(i)}| + \text{c.c.}$, where $\mu_{Q_Xg}^{(i)} = \mu_{gQ_X}^{(i)}$ and $\mu_{Q_Yg}^{(i)} = \mu_{gQ_Y}^{(i)}$ are chosen such that $\mu_{Q_Xg}^{(i)}$ has zero projection along the y axis, and $\mu_{Q_Yg}^{(i)}$ is orthogonal to it,

$$\begin{aligned}\mu_{Q_Xg}^{(i)} &= d(\cos\theta_i, 0, \sin\theta_i), \\ \mu_{Q_Yg}^{(i)} &= d(-\sin\varphi_i\sin\theta_i, \cos\varphi_i, \sin\varphi_i\cos\theta_i),\end{aligned}$$

where $d \sim 2 - 8\text{D}$ depending on the chemical environment of the porphyrins [40]. These vectors define molecular frames for each sublattice, with Cartesian unit vectors $X_i = \frac{\mu_{Q_Xg}^{(i)}}{d}$, $Y_i = \frac{\mu_{Q_Yg}^{(i)}}{d}$, and $Z_i = X_i \times Y_i$. Also, in general $(\theta_a, \varphi_a) \neq (\theta_b, \varphi_b)$, so the tilting angles distinguish the sublattices.

Interaction with a magnetic field.— Before dealing with the dipolar interactions between the different porphyrins, we consider their Zeeman interaction with a perpendicular and homogeneous magnetic field $B = (0, 0, B)$ (see Fig. 2). This implicitly assumes a separation of timescales whereby the Zeeman effect is much stronger than the interchromophoric interaction [41],

$$H^{(i)} = H_0^{(i)} - \mu_0 B \cdot (L^{(i)} + 2S^{(i)}). \quad (1)$$

Here, $H_0^{(i)} = \omega_Q(|Q_X^{(i)}\rangle\langle Q_X^{(i)}| + |Q_Y^{(i)}\rangle\langle Q_Y^{(i)}|)$ is the bare Hamiltonian of each porphyrin, $\mu_0 = 0.47\text{cm}^{-1}\text{T}^{-1}$ is the Bohr magneton, and $L^{(i)}$ and $S^{(i)}$ are the electronic orbital angular momentum and spin of the i th porphyrin. Each of the three states per molecule is a singlet state with $S^{(i)} = 0$. It is valid to regard the porphyrins as approximate rings in the $X_i Y_i$ planes occupied by 18 electrons [39, 41, 42]. This implies that the solutions to Eq. (1) are states with approximately good angular momentum quantum number $L_Z^{(i)} = \pm m$ perpendicular to the plane of the molecules at Z_i for integer m (here $\hbar = 1$). In particular, we have $L_Z^{(i)}|g^{(i)}\rangle = 0$ and $L_Z^{(i)}|Q_{\pm}^{(i)}\rangle \equiv L_Z^{(i)}(|Q_X^{(i)}\rangle \pm i|Q_Y^{(i)}\rangle)/\sqrt{2} = \pm 9|Q_{\pm}^{(i)}\rangle$, yielding $H^{(i)}|g^{(i)}\rangle = 0$ and $H^{(i)}|Q_{\pm}^{(i)}\rangle = (\omega_Q \mp \Delta_i)|Q_{\pm}^{(i)}\rangle$, where half of the Zeeman splitting is given by $\Delta_i \equiv 9\mu_0 B_z \kappa_i$, and we have used $\kappa_i \equiv z \cdot Z_i = \cos\theta_i \cos\varphi_i$. That is, under a magnetic field, the degenerate Q-band in each porphyrin splits into two Zeeman levels $|Q_{\pm}^{(i)}\rangle$ with different energies. Notice that due to TRS breaking, their coefficients in terms of the “bare” states $|Q_X^{(i)}\rangle$ and $|Q_Y^{(i)}\rangle$ are in general complex. Although not essen-

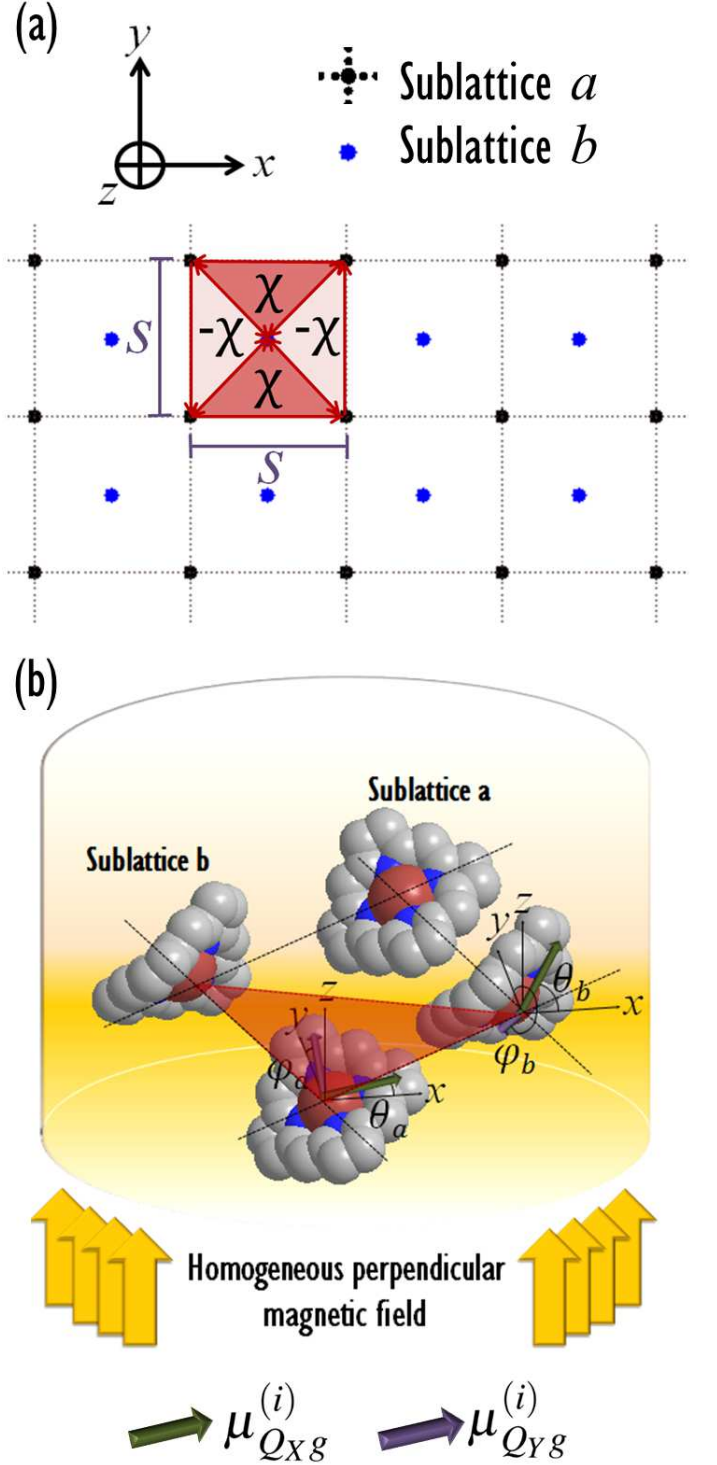


Figure 1: *Porphyrin lattice under a uniform magnetic field.* (a) The square lattice consists of porphyrins arranged into two sublattices a (black) and b (blue). A possible unit cell is a square of dimensions $s \times s$. We highlight the fluxes (Berry phases) $\pm\chi$ that the exciton obtains upon counterclockwise circulation about each of minimal three porphyrin loops. This pattern of fluxes is reminiscent to Haldane’s model, where electrons are placed in a lattice under an inhomogeneous magnetic field with no effective magnetic field per unit cell, and yet, manifest nontrivial topological properties. (b) Magnification of the upper corner of the unit cell in (a). The actual setup uses a homogeneous magnetic field. Sublattice a differs from sublattice b in the orientation angles θ_i, φ_i ($i = a, b$) of the porphyrins with respect to the x and y axes. Each porphyrin consists of two transition dipoles $\mu_{Q_Xg}^{(i)}$ and $\mu_{Q_Yg}^{(i)}$ in the plane of the molecules. The anisotropic character of dipolar interactions together with the magnetic field makes the exciton hoppings along the northeast and the northwest directions

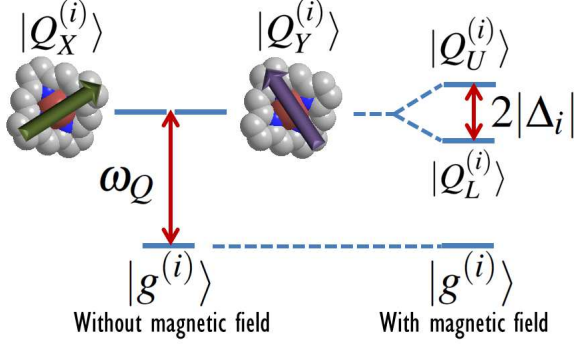


Figure 2: *(Metallo-)Porphyrin under a magnetic field.* In the absence of a magnetic field, a porphyrin can be thought of as three-level molecules with a ground state $|g^{(i)}\rangle$ and a Q-band formed by two degenerate excited states $|Q_X^{(i)}\rangle$ and $|Q_Y^{(i)}\rangle$ at an energy ω_Q . A magnetic field B breaks time-reversal symmetry, as well as the degeneracy via a Zeeman splitting $2|\Delta_i|$, yielding lower $|Q_L^{(i)}\rangle$ and upper $|Q_U^{(i)}\rangle$ eigenstates with definite angular momentum along Z_i . Here, i denotes different sublattices $i = a, b$.

tial, we simplify the model by fixing the projection of the magnetic field on both sublattices to be a constant $|\kappa_i| = \kappa \neq 0$, yielding a constant Zeeman splitting throughout $|\Delta_i| = \Delta$. There is however, a possibly different ordering of the $|Q_{\pm}^{(i)}\rangle$ states, depending on the sign of $B_z \kappa_i$. With this in mind, each porphyrin has states of energy $\omega_L \equiv \omega_Q - \Delta$ and $\omega_U \equiv \omega_Q + \Delta$, which we call the *lower* and *upper* energy states $|Q_L^{(i)}\rangle$ and $|Q_U^{(i)}\rangle$, and $(L, U) = (+, -)$ if $B_z \kappa_i > 0$ and $(L, U) = (-, +)$ otherwise. Working under a magnetic field of $|B_z| = 10$ T, this splitting attains a value of $2\Delta \sim 84 \text{ cm}^{-1}$, which is confirmed by magnetic dichroism experiments [39] (the reference reports half of the actual splitting due to isotropic averaging). It is clear from this model that other chromophores with similar electronic structure, such as metallophthalocyanines [26], can be used instead of metalloporphyrins.

Dipolar interactions between Zeeman levels.— At this point, we turn our attention to interactions between porphyrin transitions across the lattice. We are only interested in weak, “single-excitation” effects, so it is convenient to introduce the the global ground state $|G\rangle \equiv |g\rangle \cdots |g\rangle$ as well as the single-site excited states $|n_q^{(i)}\rangle \equiv |g\rangle \cdots |Q_q^{(i)}\rangle \cdots |g\rangle$, with $q = X, Y, L, U$, where every porphyrin in the lattice is in the ground state except for the porphyrin in sublattice i with coordinates ns , which is in the $|Q_q^{(i)}\rangle$ excited state [43]. Couplings between the bare porphyrin sites in the lattice are well approximated by the classical real-valued dipole-dipole interaction [44],

$$\langle n_q^{(i)} | \mathcal{J} | m_r^{(j)} \rangle \approx \frac{f}{|R_{nm}^{(ij)}|^3} \left(\mu_{Q_q}^{(i)} \cdot \mu_{Q_r}^{(j)} - 3(\mu_{Q_q}^{(i)} \cdot e_{nm}^{(ij)})(\mu_{Q_r}^{(j)} \cdot e_{nm}^{(ij)}) \right) \quad (2)$$

Here, $f = 5.04 \text{ cm}^{-1} (\text{nm}^3 / D^2)$ (we have set the index of refraction to 1), $q, r = X, Y$, and $R_{nm}^{(ij)}$ is the position vector pointing from the n th porphyrin of sublattice i to the m th porphyrin

of sublattice j , and $e_{nm}^{(ij)} = \frac{R_{nm}^{(ij)}}{|R_{nm}^{(ij)}|}$. To establish an energy scale associated with these interactions, we define $J \equiv \frac{fd^2}{s^3}$, which for $d = 3$ D and $s = 2$ nm gives $J = 5.7 \text{ cm}^{-1}$, so that $2\Delta \gg J$, the Zeeman splitting is much larger than the dipolar couplings, consistent with our assumptions. Couplings between Zeeman levels follow from Eq. (2) and the appropriate change of basis,

$$\langle n_u^{(i)} | \mathcal{J} | m_v^{(j)} \rangle = \sum_{q,r=X,Y} \langle Q_u^{(i)} | Q_q^{(i)} \rangle \langle n_q^{(i)} | \mathcal{J} | m_r^{(j)} \rangle \langle Q_r^{(j)} | Q_v^{(j)} \rangle, \quad (3)$$

where $u, v = L, U$. From the energetic considerations above, we need to include couplings within each band of $|Q_L^{(i)}\rangle$ or $|Q_U^{(i)}\rangle$ states, but not between them. Therefore, we may write a Frenkel exciton Hamiltonian for the total lattice that reads as $\mathcal{H} = \mathcal{H}_L + \mathcal{H}_U$. As an illustration, let us explicitly construct the Hamiltonian \mathcal{H}_L for the lower energy states $|Q_L^{(i)}\rangle$, or alternatively $|n_L^{(i)}\rangle$, by introducing the second quantized notation for each sublattice $a_n^\dagger |G\rangle = |n_L^{(a)}\rangle$ and $b_n^\dagger |G\rangle = |n_L^{(b)}\rangle$. Restricting the interactions to nearest neighbors (NN) and next-nearest neighbors (NNN), we have the following two-band model,

$$\begin{aligned} \mathcal{H}_L = \sum_n \left(\omega_L (a_n^\dagger a_n + b_n^\dagger b_n) \right. \\ + J_{ab,NE} (a_{n+NE}^\dagger b_n + a_{n-NE}^\dagger b_n) \\ + J_{ab,NW} (a_{n+NW}^\dagger b_n + a_{n-NW}^\dagger b_n) \\ + J_{aa,E} a_{n+E}^\dagger a_n + J_{aa,N} a_{n+N}^\dagger a_n \\ \left. + J_{bb,E} b_{n+E}^\dagger b_n + J_{bb,N} b_{n+N}^\dagger b_n \right) + \text{c.c.}, \quad (4) \end{aligned}$$

where the couplings are given by $J_{ij,V} \equiv \langle (n+V)_L^{(i)} | \mathcal{J} | n_L^{(j)} \rangle = \langle (n-V)_L^{(i)} | \mathcal{J} | n_L^{(j)} \rangle$, and the vectors V for the north, east, northeast, and northwest directions are $N = (0, 1, 0)$, $E = (1, 0, 0)$, $NE = \frac{1}{2}(1, 1, 0)$, and $NW = \frac{1}{2}(-1, 1, 0)$. The analogous Hamiltonian \mathcal{H}_U can be similarly constructed using the states $|Q_U^{(i)}\rangle$ or $|n_U^{(i)}\rangle$. It is easy to check that the NNN couplings $J_{ii,V}$ are real-valued, but that the NN couplings $J_{ab,V}$ are complex-valued in general due to the overlaps $\langle Q_u^{(i)} | Q_q^{(i)} \rangle$ associated with the change of basis (see Eq. (3)). We note that complex phases in these couplings do not represent physical observables on their own, as they can be modified via gauge transformations. Yet, the Berry phases accumulated in closed loops, and in particular those obtained by encircling the minimal three porphyrins loops are gauge invariant modulo 2π and therefore, have observable consequences. Fig. 1 shows that in each unit cell, two of the counterclockwise loops yield a phase $\chi \equiv \arg(J_{ab,NW}^* J_{aa,NE} J_{ab,E}) = -\arg(J_{ab,NW} J_{ab,E})$ and the other two yield the opposite phase $\arg(J_{ab,SE} J_{ba,SW} J_{aa,N}) = -\chi$. A peculiar feature of dipolar interactions between the tilted porphyrins is its anisotropic character which renders $\arg(J_{ab,NE})$

different from $\arg(J_{ab,NW})$, except for a measure-zero set of critical orientations, and therefore keeps χ finite for every set of tilting angles as long as the magnetic field is on. This observation is also at the core of recent work on topological phases in dipolar spins for optical lattices [45, 46]. Thus, Eq. (4) has the same structure as the Hamiltonian for electrons in a lattice under a perpendicular and *inhomogeneous* magnetic field threading net fluxes $\pm\chi$ across the minimal loops, but a net zero magnetic flux per unit cell, and therefore, across the lattice. Let us summarize what we have done so far: we have constructed a model where Frenkel excitons (quasiparticles with no net charge) under a homogenous magnetic field behave as if they were electrons (particles with charge) in an inhomogeneous magnetic field. Hence, this model is a square lattice version of Haldane's honeycomb problem, and therefore, expected to exhibit nontrivial topological properties, in particular, chiral Frenkel exciton edge states which are robust against disorder [47]. This realization is the main finding of the article.

Discussion

Upon fixing the Zeeman splitting $2\Delta = |B_z|\kappa$, the unit cell distance s , and transition dipole moment strength d , there is a two-dimensional parameter space which is left to be explored by varying the tilting angles θ_a and θ_b (the possible values of φ_a and φ_b are fixed by κ). These parameters suffice to provide a topological characterization of \mathcal{H}_v via the Chern numbers \mathcal{C}_v for $v = L, U$ (see Supplementary Information for details) [20, 48]. The physical meaning of \mathcal{C}_v is the following: Its sign denotes the chirality of the edge states (in our convention, positive for clockwise and negative for counterclockwise); its magnitude is equal to the (integer) number of edge states per value of quasimomentum (given open boundary conditions (OBC) along one axis).

A computational exploration of the parameter space reveals that $\mathcal{C}_v = \pm 1$ for every tilting configuration that respects the specified constraints, except for a measure zero set of parameters which yields $\mathcal{C}_v = 0$, when the two sublattices become identical at the critical values $\theta_b = \pm\theta_a, \pi \pm \theta_a$, and the gap between the two bands in each \mathcal{H}_v closes. Additionally, we can see that $\langle n_L^{(i)} | J | m_L^{(j)} \rangle = \langle n_U^{(i)} | J | m_U^{(j)} \rangle^*$, so that every minimal loop that features a flux χ in \mathcal{H}_L (see previous section), features the opposite flux $-\chi$ in \mathcal{H}_U , implying that $\mathcal{C}_L = -\mathcal{C}_U$. Therefore, both clockwise and counterclockwise edge currents show up in every topologically nontrivial configuration, except that they come at different energies separated by $\sim 2\Delta$. Yet, it is possible to control the energy level ordering of these chiral currents by tuning the direction of the magnetic field, as our numerical studies show that $\mathcal{C}_L = -\text{sgn}(B_z)$. This picture contrasts radically with that of the integer QHE in a two-dimensional electron gas in the absence of a lattice, where the direction of the magnetic field imposes a fixed direction of cyclotron motion of the electrons and therefore, also the chirality of all the edge currents. As an illustration of these ideas, Fig. 3 shows the topological phase diagram for the $\kappa = \frac{1}{2}, B_z > 0$ case. Given

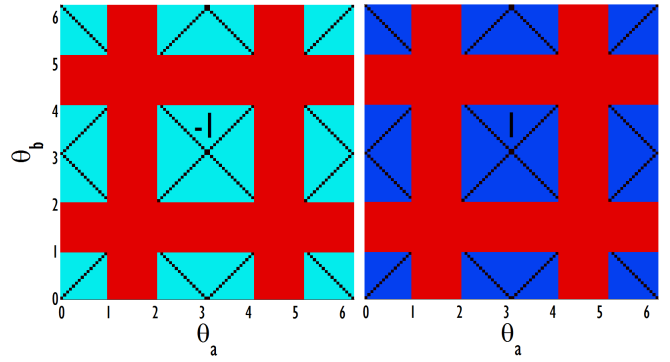


Figure 3: *Phase diagram of exciton topological phases.* We fix $\kappa = |\cos\theta_i \cos\varphi_i| = \frac{1}{2}$, the projection of the magnetic field $B_z > 0$ with the porphyrin rings and we study the resulting topological phases as a function of the tilting angles θ_i ($\pm\varphi_i$ is fixed by κ , $i = a, b$). Red regions are parameters for which values of θ_i and φ_i cannot yield $\kappa = \frac{1}{2}$, and therefore, are not considered. (a) and (b) are diagrams for the upper and lower energy exciton Hamiltonians \mathcal{H}_χ ($v = L, U$), respectively. Light and dark blue regions denote topologically nontrivial phases with Chern number \mathcal{C}_v equal to -1 and 1 , exhibiting edge states with counterclockwise and clockwise exciton currents, respectively. Switching the direction of the magnetic field to $B_z < 0$ inverts these chiralities. Black lines correspond to topologically trivial phases with $\mathcal{C}_v = 0$ and are located along the critical parameters $\theta_b = \pm\theta_a, \pi \pm \theta_a$, where the two sublattices become identical and the gaps of the respective Hamiltonians vanish.

κ and the fact that $\cos\theta_i, \cos\varphi_i \in [-1, 1]$, we must restrict $\theta_i \in [-\arccos\kappa, \arccos\kappa] \cup [\pi - \arccos\kappa, \pi + \arccos\kappa]$. The rest of the angles violate the condition of fixed $|\kappa_i| = \kappa$, but a fraction of them still contains topologically nontrivial phases. The characterization of this precise fraction is beyond the scope of this article, but will be explored in the extension of this work.

Let us be more explicit by considering a particular point $(\theta_a, \varphi_a) = (-\frac{\pi}{3}, 0)$ and $(\theta_b, \varphi_b) = (0, \frac{\pi}{3})$ of this phase diagram where $-\kappa_a = \kappa_b = \kappa = \frac{1}{2}$. We refer the reader to Fig. 4, which is organized in a top and a bottom panels (a) and (b), each of them containing three parts. We show results for \mathcal{H}_L , with the conclusions for \mathcal{H}_U being analogous except for opposite chirality of edge currents (energies and dipoles are plotted in units of J and d). The upper panel refers to the ideal case where the tilting angles of the porphyrins are placed exactly at the mentioned values. The lower panel offers a specific realization of disorder where each of the site angles has been randomized with Gaussian noise with 0.13π standard deviation about the ideal values. The left panels show the current density for a particular eigenstate of \mathcal{H}_L under OBC. These currents are concentrated along the edges of the material, so they correspond to exciton edge states and they flow clockwise, consistent with $\mathcal{C}_L = -1$. Interestingly, in the disordered lattice, regardless of the tilting randomization, the edge current and its chirality are still preserved. In order to accentuate this effect, we add a potential barrier at the left corner of the lattice, simulating an obstacle. The exciton current simply circumvents the obstacle, keeping its delocalization throughout, hence, exemplifying the properties of topological protection.

We have shown lattices with approximately 200 porphyrins, corresponding to a reasonable number of molecules that remain coherently coupled at cryogenic temperatures [49]; this number might even be a lower bound, as coherence size is limited by coupling to vibrations and disorder, but the latter is somehow circumvented in these topological systems. The center panels offer the energy diagrams of the respective lattices under OBC along y and periodic boundary conditions (PBC) along x . For the ideal lattice, this corresponds to two bulk bands as a function of quasimomentum k_x together with edge states that span the gap between the latter from $E \approx -2J$ to $2J$. The dispersion of the edge states is positive and negative, corresponding to currents at the bottom and top edges of the lattice. Note that these states of opposite dispersion merge at $k_x = 0$ with the bulk bands. The analogous band diagram is unavailable for the disordered lattice due to lack of translational symmetry, so we simply collapse all the eigenenergies in the same line. A study of the eigenstates reveals that the eigenstates between $E \approx -0.8J$ and $0.4J$ exhibit mostly edge character. We comment that, in fact, edge states seem to survive up to a large amount of disorder, namely, with noise distributed at $\frac{\pi}{6}$ standard deviation. Finally, the right panels show the linear absorption spectra of the lattice with OBCs along both directions x and y . In analogy with J- and H-aggregates, most of their oscillator strength is concentrated in relatively few bulk eigenstates in the ideal lattice, although neither at top or bottom of the bands, as opposed to the simple quasi-one-dimensional scenario [49]. This renders the edge states in the top panel mostly dark, with the brightest edge state absorbing only 2.7% of the highest absorption peak in the spectrum. This fact is consistent with the observation that, in the dipole approximation, only states with $k_x = 0$ are bright, but there are no such states located at the edge in our particular model. Counterintuitively, moderate amounts of disorder provide a solution to this problem, as the edge states in this lattice borrow enough oscillator strength from the original bulk states to yield peaks in the absorption spectrum that are more experimentally accessible [7], with some edge absorption peaks attaining intensities of about 26% of the highest bulk bands. Hence, linear absorption spectra provide a coarse signature of the edge states although no actual confirmation of their topological character. In order to experimentally probe the latter, we envision the use of near field optical microscopy, where a metal tip locally creates excitons at the edge of the lattice and spatially resolved fluorescence is used to detect the chirality of the resulting exciton currents [50]. This phenomenology could also be inferred using far field microscopy, albeit at a coarser spatial resolution [51]. The detailed proposal for the experimental preparation and detection of the edge exciton currents is a delicate subject on its own, and will be reported in an extension of this work. Similarly, as noted at the beginning of the article, we have omitted the discussion of interactions between excitons and molecular vibrations, regarding them as weak compared to the coupling J . Assuming a thermal scale $k_B T$ for the former, where k_B is Boltzmann's constant and T is the temperature, we require the hierarchy of energy scales $k_B T \ll J \ll 2\Delta$, which amounts to cryogenic values of $T \approx 4$ K, given the values of J and 2Δ in this article.

We emphasize that the restriction to cryogenic temperatures is not a fundamental one. It arises from the modest values of Zeeman splitting 2Δ attained at realistic magnetic fields, and not from J , which can assume large values upon appropriate chemical functionalization [52]. Hence, if 2Δ can be enhanced otherwise (i.e., via optical dressing), the domain validity of the model can be pushed to much higher temperatures. For arbitrary exciton-vibrational couplings, the current model needs to be adapted, and at present, it is not clear under which general conditions will topologically non-trivial phases survive, as vibrations might suppress them if they serve as a thermal dephasing bath, but may also sustain them nontrivially if they act as a non-Markovian one.

Summary and Conclusions

The present article introduces the concepts of topological phases to the field of molecular excitonics. It does so by explicitly constructing a topologically nontrivial model for Frenkel excitons in a two-dimensional lattice of porphyrins. Important ingredients of the model are the presence of two orbitally polarized excitons per porphyrin, the interaction of the lattice with a perpendicular magnetic field, the anisotropy of dipolar interactions between excitons, and the two-sublattice configuration of tilted porphyrins, yielding two pairs of exciton energy bands. The proposed system is a variant of the Haldane model, yielding one-way exciton edge states that are robust against disorder, as we have shown by calculations of topological invariants of the resulting energy bands as well as by explicit simulations of finite lattices. An experimental signature of these edge states is given by linear absorption spectra, although the experimental confirmation of their topological character requires more careful experiments, which will be proposed elsewhere.

We believe that our work is just one of many examples yet to be studied of a new pool of strategies to engineer robust "exciton wires" that can efficiently transport light harvested energy. Among some specific future directions, we plan to explore whether the coupling of excitons with various spatially shaped electromagnetic fields such as plasmons and optical cavities renders topologically nontrivial motion of excitons. Furthermore, connections between this work and theories of TRS breaking in quantum transport remain to be explored [53, 54]. Another intriguing extension of this work is the TRS version of the model, where no magnetic field is present. Regarding the Q-band of each porphyrin as a pseudospin, the anisotropy of the dipolar couplings may be regarded as a pseudospin-orbit coupling, yielding excitonic TI analogues, or more precisely, to analogues of topological crystalline insulators, which are a new class of materials where orbital degrees of freedom together with spatial symmetries of the lattice render topologically nontrivial band structures [55, 56]. We hope to have convinced the reader that topological excitonics is an exciting frontier of soft condensed matter and materials physics research.

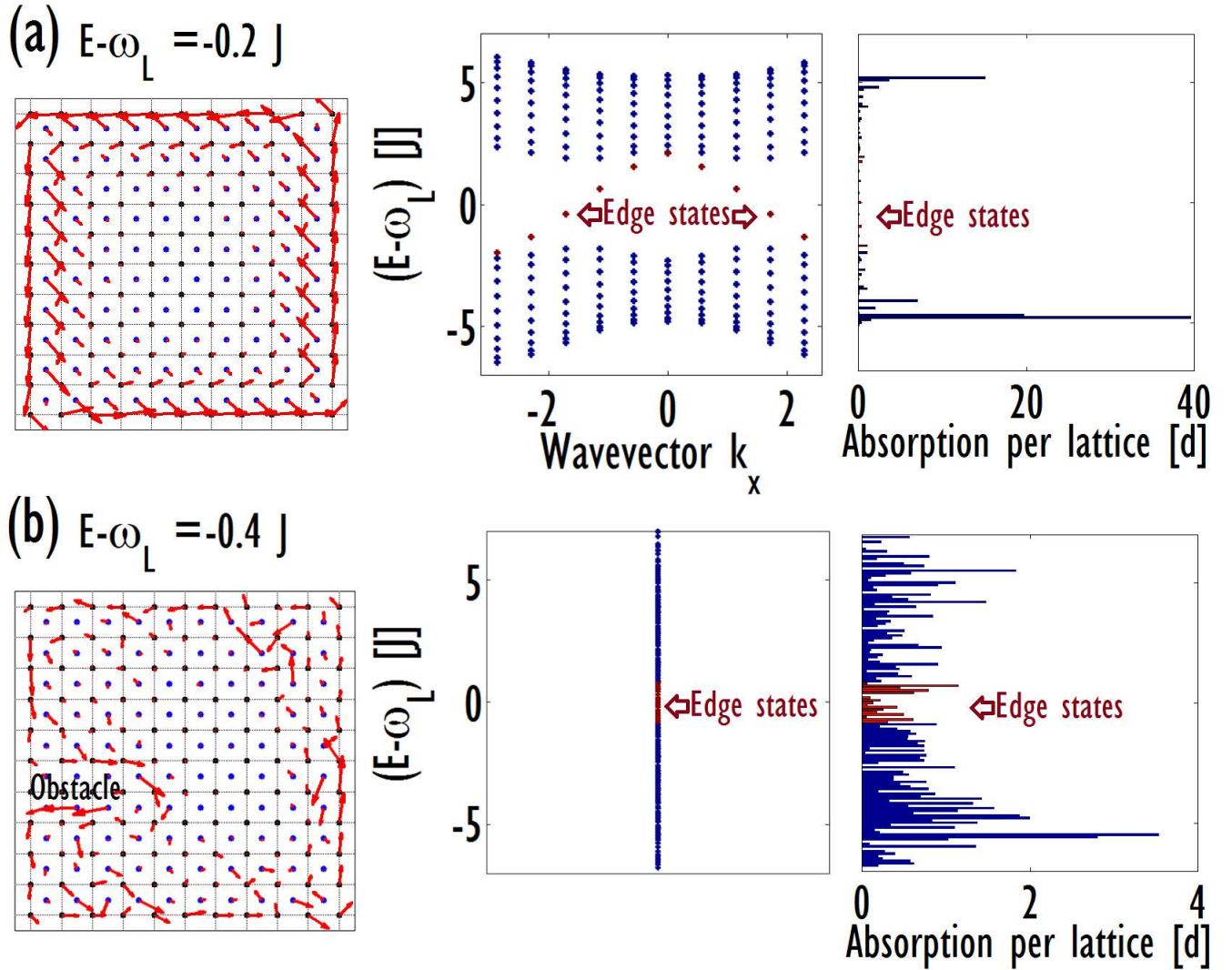


Figure 4: *Eigenstates of the lower energy Hamiltonian \mathcal{H}_L for porphyrin tilting angles $(\theta_a, \varphi_a) = (-\frac{\pi}{3}, 0)$ and $(\theta_b, \varphi_b) = (0, \frac{\pi}{3})$ and magnetic field $B_z > 0$. These parameters yield a $\mathcal{C}_L = -1$ phase, which exhibits counterclockwise edge currents. (a) Ideal lattice without disorder. The left panel shows the current density for a particular edge state. The center panel depicts the band diagram with bulk (blue) and edge (red) states. The positive and negative dispersion for the edge states correspond to right and left moving states which are localized at the lower and upper edges of the sample. The right panel shows the absorption spectrum of the lattice, indicating that most of the oscillator strength is primarily concentrated in a few bulk states. (b) The analogous panels for a disordered lattice, where the tilting angles for each porphyrin site is randomized with noise distributed at 0.13π standard deviation. Additionally, an obstacle (potential barrier) is added on the left hand corner of the lattice. Note that the edge current density persists with disorder, and in fact, circumvents the obstacle, remaining delocalized across the edge. In the center panel, we show the corresponding density of states, highlighting the region of energy where the states still have a substantial edge character. The right panel shows the absorption spectrum, where the disorder redistributes the oscillator strength of the ideal lattice. The edge states borrow enough oscillator strength to be measured experimentally in a linear absorption experiment.*

Supplementary Information

Topological characterization of the lattice Hamiltonian \mathcal{H}_L .— By imposing Periodic Boundary Conditions (PBC) along x and y , \mathcal{H}_L can be rewritten in quasimomentum k space using the operators $a_k^\dagger = \frac{1}{\sqrt{N_x N_y}} \sum_n a_n^\dagger e^{-ik \cdot n}$ and $b_k^\dagger = \frac{1}{\sqrt{N_x N_y}} \sum_n b_n^\dagger e^{-ik \cdot n}$, where N_x and N_y are the number of unit cells along the x and y directions, and $k = (k_x, k_y)$ can take

values in the Brillouin zone $-\pi \leq k_x, k_y < \pi$ in discrete steps of $\Delta k_x = \frac{2\pi}{N_x}$ and $\Delta k_y = \frac{2\pi}{N_y}$, respectively. In terms of these operators, Eq. (4) becomes $\mathcal{H}_L = \sum_k (a_k^\dagger \ b_k^\dagger) H(k) (a_k \ b_k)^T$, where $H(k) = d(k) \cdot \sigma + f(k)I$ describes a two-band model. Here, $\sigma = (\sigma_x, \sigma_y, \sigma_z)$ and I are the vector of Pauli spin matrices and the two-by-two identity matrix, and $d(k) = (d_x(k), d_y(k), d_z(k))$ and $f(k)$ are a k dependent vector and

scalar given by,

$$d_x(k) = A_1 \cos\left(\frac{k_x + k_y}{2}\right) + A_2 \cos\left(\frac{k_x - k_y}{2}\right), \quad (5a)$$

$$d_y(k) = B_1 \cos\left(\frac{k_x + k_y}{2}\right) + B_2 \cos\left(\frac{k_x - k_y}{2}\right), \quad (5b)$$

$$d_z(k) = C_1 \cos(k_x) + C_2 \cos(k_y), \quad (5c)$$

$$f(k) = D_1 \cos(k_x) + D_2 \cos(k_y), \quad (5d)$$

where $A_1 = 2\Re J_{ab,NE}$, $A_2 = 2\Re J_{ab,NW}$, $B_1 = -2\Im J_{ab,NE}$, $B_2 = -2\Im J_{ab,NW}$, $C_1 = J_{aa,E} - J_{bb,E}$, $C_2 = J_{aa,N} - J_{bb,N}$, $D_1 = J_{aa,E} + J_{bb,E}$, and $D_2 = J_{aa,N} + J_{bb,N}$ (see main text for the definitions of these coupling terms). Using this parametrization, one can readily compute the Chern number \mathcal{C}_L , a topological invariant that, due to the bulk-edge correspondence [20], yields the (integer) number of edge states per quasimomen-

tum under Open Boundary Conditions (OBC) lying in the gap of the spectrum of \mathcal{H}_L or alternatively $H(k)$, whose energy bands are given by,

$$\varepsilon(k) = f(k) \pm |d(k)|. \quad (6)$$

Defining the unit vector $\hat{d}(k) = \frac{d(k)}{|d(k)|}$, \mathcal{C}_L can be calculated as an integral in k space [20, 48],

$$\mathcal{C}_L = \int_{-\pi}^{\pi} dk_x \int_{-\pi}^{\pi} dk_y \mathcal{B}(k_x, k_y). \quad (7)$$

where the Berry curvature in terms of $\hat{d}(k)$ is given by $\mathcal{B} = \frac{1}{4\pi} \hat{d} \cdot (\partial_{k_x} \hat{d} \times \partial_{k_y} \hat{d})$. The simplicity of the parametrization in Eqs. (5a)–(5d) affords an analytical expression for \mathcal{C}_L ,

$$\begin{aligned} \mathcal{C}_L &= \frac{\text{Numerator}}{\text{Denominator}}, \\ \text{Numerator} &= (A_2 B_1 - A_1 B_2) [C_1 \cos(2k_x) + (C_1 - C_2)(-3 + 2\cos(k_x)\cos(k_y)) - C_2 \cos(2k_y)], \\ \text{Denominator} &= 32\pi \{ [C_1 \cos(k_x) + C_2 \cos(k_y)]^2 + \frac{1}{2} [(A_2^2 + B_2^2)(1 + \cos(k_x - k_y)) \\ &\quad + 2(A_1 A_2 + B_1 B_2)(\cos(k_x) + \cos(k_y)) + (A_1^2 + B_1^2)(1 + \cos(k_x + k_y))] \}^{3/2}. \end{aligned} \quad (8)$$

The sign of \mathcal{C}_L indicates the chirality of the edge state and topologically nontrivial phases are characterized by a nonvanishing C_L .

A word of caution follows about the correct interpretation of \mathcal{C}_L in the context of this exciton problem, besides the one already given. First, were \mathcal{H}_L to describe an electronic rather than an exciton problem, not every band structure given by Eq. (6) satisfies the condition of an electronic insulator: due to the k -dependent offset $f(k)$, there is not always an gap where one can place the Fermi energy such that it does not cross any of the bulk bands. This issue deteriorates topological protection allowing scattering into the bulk. However, for the cases that qualify as an insulator, such as the example described in the main text, \mathcal{H}_L represents a Chern insulator which exhibits a quantized transverse conductance $\frac{e^2}{h} \mathcal{C}_L$ (e is charge of an electron, and h is Planck's constant) under a weak voltage bias, giving an experimental interpretation to the meaning of \mathcal{C}_L [48]. Our case is different as we are limiting ourselves to single excitation effects, rather than considering a macroscopic occupation of the states, as in an actual electronic insulator, and the occupation of the bands occurs through light and not through a difference in electrochemical potential. Yet, it is an intriguing problem to find an excitonic observable that directly corresponds to \mathcal{C}_L . One could imagine designing a protocol that occupies the edge states and not the bulk bands,

and which applies a bias potential to the excitons via, say, mechanical strain [57]. The measurement of an exciton current in this situation would be related to \mathcal{C}_L . As noted in the main text, a more careful description of such an experimental protocol involving near field spectroscopic techniques will be defined in the extension of this work, so for now, we will content ourselves with the first interpretation of \mathcal{C}_L in terms of the number of edge states.

Even though everything in this section referred to \mathcal{H}_L , the analogous conclusions apply to \mathcal{H}_U . In fact, one can easily show that Eq. (8) is also valid for C_U provided the corresponding dipolar couplings are used.

Symmetries of \mathcal{C}_v .— In the text, we argued that $\mathcal{C}_L = -\mathcal{C}_U$. This claim can be restated as C_v changing sign upon switching the + and – labels, $\{|Q_+^{(i)}\rangle, |Q_-^{(i)}\rangle\} \leftrightarrow \{|Q_-^{(i)}\rangle, |Q_+^{(i)}\rangle\}$. By keeping track of the various matrix elements, we can see that C_v also reverses sign upon the transformation $\kappa_i \leftrightarrow -\kappa_i$ across both sublattices. However, inverting the projection of the magnetic field on the porphyrins, $\kappa_i \leftrightarrow -\kappa_i$, also reassigns the upper and lower energy states $|Q_L^{(i)}\rangle$ and $|Q_U^{(i)}\rangle$ between $|Q_+^{(i)}\rangle$ and $|Q_-^{(i)}\rangle$, switching + and – labels. Hence, the value of \mathcal{C}_L (and consequently, of \mathcal{C}_U) is fixed across tilting configurations, and by computation seen to correspond to $\mathcal{C}_L = -1$ for $B_z > 0$. Since B_z also switches + and –, $\mathcal{C}_L = 1$ for $B_z < 0$.

- [1] A.S. Davydov. *Theory of molecular excitons*. McGraw-Hill, 1962.
- [2] B. A. Gregg. Excitonic solar cells. *J. Phys. Chem. B*, 107(20):4688–4698, 2003.
- [3] G. D. Scholes and G. Rumbles. Excitons in nanoscale systems. *Nat. Materials*, 5:683–696, 2006.
- [4] S. K. Saikin, A. Eisfeld, S. Valleau, and A. Aspuru-Guzik. Photonics meets excitonics: natural and artificial molecular aggregates. *Nanophotonics*, 2:21–38, 2013.
- [5] B. Kippelen and J.-L. Bredas. Organic photovoltaics. *Energy Environ. Sci.*, 2:251–261, 2009.
- [6] C. Brabec, U. Scherf, and V. Dyakonov, editors. *Organic Photovoltaics: Concepts and Realization*. Springer, 2003.
- [7] H. Fidler, J. Knoester, and D. A. Wiersma. Optical properties of disordered molecular aggregates: A numerical study. *J. Chem. Phys.*, 95(11):7880–7890, 1991.
- [8] M. Mohseni, P. Rebentrost, S. Lloyd, and A. Aspuru-Guzik. Environment-assisted quantum walks in photosynthetic energy transfer. *J. Chem. Phys.*, 129:174106, 2008.
- [9] M. B. Plenio and S. F. Huelga. Dephasing-assisted transport: quantum networks and biomolecules. *New J. Phys.*, 10:113019, 2008.
- [10] J. Cao and R. J. Silbey. Optimization of exciton trapping in energy transfer processes. *J. Phys. Chem. A*, 113:13825–13838, 2009.
- [11] D. Yoshioka. *The Quantum Hall Effect*. Springer, 1998.
- [12] B. I. Halperin. Quantized hall conductance, current-carrying edge states, and the existence of extended states in a two-dimensional disordered potential. *Phys. Rev. B*, 25:2185–2190, 1982.
- [13] Z. Wang, Y. Chong, J. D. Joannopoulos, and M. Soljacic. Observation of unidirectional backscattering-immune topological electromagnetic states. *Nature*, 461:772–775, October 2009.
- [14] M. Hafezi, E. A. Demler, M. D. Lukin, and J. M. Taylor. Robust optical delay lines with topological protection. *Nat. Phys.*, 7:907–912, November 2011.
- [15] M. C. Rechtsman, J. M. Zeuner, Y. Plotnik, Y. Lumer, D. Podolsky, F. Dreisow, S. Nolte, M. Segev, and A. Szameit. Photonic floquet topological insulators. *Nature*, 496:196–200, April 2013.
- [16] M. Hafezi, S. Mittal, J. Fan, A. Migdall, and J. M. Taylor. Imaging topological edge states in silicon photonics. *Nat. Photon.*, 7:1001–1005, December 2013.
- [17] A. B. Khanikaev, S. Hossein Mousavi, W. K. Tse, M. Kargarian, A. H. MacDonald, and G. Shvets. Photonic topological insulators. *Nature Materials*, 12:233–239, March 2013.
- [18] M. Z. Hasan and C. L. Kane. *Colloquium: Topological insulators*. *Rev. Mod. Phys.*, 82:3045–3067, Nov 2010.
- [19] X. Qi and S.-C. Zhang. Topological insulators and superconductors. *Rev. Mod. Phys.*, 83:1057–1110, 2011.
- [20] B. A. Bernevig. *Topological Insulators and Topological Superconductors*. Princeton University Press, 2013.
- [21] D. Kong and Y. Cui. Opportunities in chemistry and materials science for topological insulators and their nanostructures. *Nat. Chem.*, (3):845–849, 2011.
- [22] Z. F. Wang, Ninghai Su, and Feng Liu. Prediction of a two-dimensional organic topological insulator. *Nano Letters*, 13(6):2842–2845, 2013.
- [23] Z. F. Wang, Z. Liu, and F. Liu. Organic topological insulators in organometallic lattices. *Nat. Comm.*, 4, February 2013.
- [24] Z. Liu, Z. F. Wang, J. W. Mei, Y. S. Wu, and F. Liu. Flat Chern band in a two-dimensional organometallic framework. *Phys. Rev. Lett.*, 110:106804, Mar 2013.
- [25] Z. F. Wang, Zheng Liu, and Feng Liu. Quantum anomalous hall effect in 2d organic topological insulators. *Phys. Rev. Lett.*, 110:196801, May 2013.
- [26] Kadish K. M., Smith K. M., and Guillard R., editors. *Handbook of Porphyrin Science*. World Scientific, 2010.
- [27] D. Kim, editor. *Multiporphyrin Arrays: Fundamentals and Applications*. Pan Stanford Publishing, 2012.
- [28] H. Imahori and S. Fukuzumi. Porphyrin- and fullerene-based molecular photovoltaic devices. *Adv. Func. Mat.*, 14(6):525–536, 2004.
- [29] M. Victoria Martinez-Diaz, Gema de la Torre, and Tomas Torres. Lighting porphyrins and phthalocyanines for molecular photovoltaics. *Chem. Commun.*, 46:7090–7108, 2010.
- [30] M. G. Walter, A. B. Rudine, and C. C. Wamser. Porphyrins and phthalocyanines in solar photovoltaic cells. *J. of Porphyrins and Phthalocyanines*, 14(09):759–792, 2010.
- [31] K. Suto, S. Yoshimoto, and K. Itaya. Two-dimensional self-organization of phthalocyanine and porphyrin: Dependence on the crystallographic orientation of au. *J. Am. Chem. Soc.*, 125(49):14976–14977, 2003.
- [32] E. Barrera, D. G. de Oteyza, H. Dosch, and Y. Wakayama. 2d supramolecular self-assembly of binary organic monolayers. *ChemPhysChem*, 8(13):1915–1918, 2007.
- [33] J. Brede, M. Linares, S. Kuck, J. Schwobel, A. Scarfato, S. H. Chang, G. Hoffmann, R. Wiesendanger, R. Lensen, P. H. J. Kouwer, J. Hoogboom, A. E. Rowan, M. Broring, M. Funk, S. Stafstrom, F. Zerbetto, and R. Lazzaroni. Dynamics of molecular self-ordering in tetraphenyl porphyrin monolayers on metallic substrates. *Nanotechnology*, 20(27):275602, 2009.
- [34] A. Gao, X. Miao, J. Liu, P. Zhao, J. Huang, and W. Deng. Two-dimensional self-assembly of a porphyrin-polypyridyl ruthenium(ii) hybrid on hcp surface through metal-ligand interactions. *ChemPhysChem*, 11(9):1951–1955, 2010.
- [35] T. Birnbaum, T. Hahn, C. Martin, J. Kortus, M. Fronk, F. Lungwitz, D. R. T. Zahn, and G. Salvan. Optical and magneto-optical properties of metal phthalocyanine and metal porphyrin thin films. *J. Phys. Cond. Matt.*, 26(10):104201, 2014.
- [36] V. Feyer, M. Graus, P. Nigge, M. Wiesner, R.G. Acres, C. Wiemann, C.M. Schneider, A. Scholl, and F. Reinert. Adsorption geometry and electronic structure of iron phthalocyanine on Ag surfaces: A {LEED} and photoelectron momentum mapping study. *Surf. Sci.*, 621(0):64 – 68, 2014.
- [37] S. Maier, L. A. Fendt, L. Zimmerli, T. Glatzel, O. Pfeiffer, F. Diederich, and E. Meyer. Nanoscale engineering of molecular porphyrin wires on insulating surfaces. *Small*, 4(8):1115–1118, 2008.
- [38] A. Scarfato, S. H. Chang, S. Kuck, J. Brede, G. Hoffmann, and R. Wiesendanger. Scanning tunneling microscope study of iron(ii) phthalocyanine growth on metals and insulating surfaces. *Surf. Sci.*, 602(3):677 – 683, 2008.
- [39] Malley M., Feher G., and Mauzerall D. The zeeman effect in porphyrins. *J. Mol. Spectrosc.*, 26(3):320 – 334, 1968.
- [40] D. Villamaina, S. V. Bhosale, S. J. Langford, and E. Vauthey. Excited-state dynamics of porphyrin-naphthalenediimide-porphyrin triads. *Phys. Chem. Chem. Phys.*, 15:1177–1187, 2013.
- [41] Canters G. W. and van der Waals J. H. *High-Resolution Zeeman Spectroscopy of Metalloporphyrins*, volume 3 of *The Porphyrins*, chapter 12, pages 531–582. Academic Press, 1978.

- [42] Rodriguez J. J. and Mukamel S. Zeeman shift of two-dimensional optical signals of mg-porphyrin dimers with circularly polarized beams. *J. Chem. Phys.*, 137(20):205102, 2012.
- [43] V. May and O. Kuhn. *Charge and Energy Transfer Dynamics in Molecular Systems*. Wiley-VCH, 2004.
- [44] Valkunas L. van Amerongen H. and van Grondelle R. *Photo-synthetic Excitons*. World Scientific, 2000.
- [45] N. Y. Yao, C. R. Laumann, A. V. Gorshkov, S. D. Bennett, E. Demler, P. Zoller, and M. D. Lukin. Topological flat bands from dipolar spin systems. *Phys. Rev. Lett.*, 109:266804, 2012.
- [46] N. Y. Yao, A. V. Gorshkov, C. R. Laumann, A. M. Läuchli, J. Ye, and M. D. Lukin. Realizing fractional chern insulators in dipolar spin systems. *Phys. Rev. Lett.*, 110:185302, 2013.
- [47] F. D. M. Haldane. Model for a quantum hall effect without landau levels: Condensed-matter realization of the "parity anomaly". *Phys. Rev. Lett.*, 61:2015–2018, 1988.
- [48] D. J. Thouless, M. Kohmoto, M. P. Nightingale, and M. den Nijs. Quantized hall conductance in a two-dimensional periodic potential. *Phys. Rev. Lett.*, 49:405–408, 1982.
- [49] J. Knoester. Modeling the optical properties of excitons in linear and tubular j-aggregates. *Int. J. Photoenergy*, 2006(61364):1–10, 2006.
- [50] E. J. Sánchez, L. Novotny, and X. S. Xie. Near-field fluorescence microscopy based on two-photon excitation with metal tips. *Phys. Rev. Lett.*, 82:4014–4017, 1999.
- [51] G. M. Akselrod, P. B. Deotare, N. J. Thompson, J. Lee, W. A. Tisdale, M. A. Baldo, V. M. Menon, and V. Bulovic. Visualization of exciton transport in ordered and disordered molecular solids. *Nat. Comm.*, 5, April 2014.
- [52] D. Sheberla, L. Sun, M. A. Blood-Forsythe, S. Er, C. R. Wade, C. K. Brozek, A. Aspuru-Guzik, and M. Dinca. High electrical conductivity in ni₃(2,3,6,7,10,11-hexaiminotriphenylene)₂, a semiconducting metal-organic graphene analogue. *J. Am. Chem. Soc.*, 0(0):null, 0.
- [53] Z. Zimborás, M. Faccin, Z. Kádár, J. D. Whitfield, B. Lanyon, and J. Biamonte. Quantum transport enhancement by time-reversal symmetry breaking. *Sci. Rep.*, 3:1–6, June 2013.
- [54] D. Lu, J. D. Biamonte, J. Li, H. Li, T. H. Johnson, V. Bergholm, M. Faccin, Z. Zimborás, R. Laflamme, J. Baugh, and S. Lloyd. Chiral quantum walks. *ArXiv e-prints*, May 2014.
- [55] L. Fu. Topological crystalline insulators. *Phys. Rev. Lett.*, 106:106802, 2011.
- [56] T. H. Hsieh, H. Lin, J. Liu, W. Duan, A. Bansil, and L. Fu. Topological crystalline insulators in the SnTe material class. *Nat. Comm.*, 3, 2012.
- [57] J. Feng, X. Qian, C.-W. Huang, and J. Li. Strain-engineered artificial atom as a broad-spectrum solar energy funnel. *Nature Photonics*, 6:866–872, December 2012.

Acknowledgements

J.Y.Z. is grateful to Dr. I. Kassal for introducing him to the topic of topological phases, to Prof. B. Halperin and Dr. X. Andrade for discussions, and to Prof. O. Starykh for kindly sharing his notes on the subject. All the authors would like to thank Prof. C. Laumann for discussions at the early stages of the project. J.Y.Z. and A.A.G. are supported by an Energy Frontier Research Center funded by the US Department of Energy, Office of Science, Office of Basic Energy Sciences under Award Number DESC0001088. N.Y. acknowledges support from DOE (FG02-97ER25308). Finally, S.K.S. and A.A.-G. are supported by the Defense Threat Reduction Agency grant HDTRA1-10-1-0046.